Large-scale spatial variability in loess landforms and their evolution, Luohe River Basin, Chinese Loess Plateau

Hong Wei [a,b,c,d*], Liyang Xiong [a,c,d], Fei Zhao [a,c,d], Guoan Tang [a,c,d], Stuart N. Lane [b]

[a] Key Laboratory of Virtual Geographic Environment (Nanjing Normal University), Ministry of Education, Nanjing 210023, China

[b] Institute of Earth Surface Dynamics (IDYST), University of Lausanne, Lausanne 1015, Switzerland

[c] School of Geography, Nanjing Normal University, Nanjing 210023, China

[d] Jiangsu Centre for Collaborative Innovation in Geographical Information Resource Development and Application, Nanjing 210023, China

* Corresponding author at: School of Geography, Nanjing Normal University, Nanjing 210023, China. E-mail address: weihongis@njnu.edu.cn (H. Wei).

Abstract: Loess landform variability across large spatial extents needs to be analyzed to understand the formation and evolution of loess landscapes. This is becoming increasingly possible via the automated analysis of remotely-sensed data. Here, we quantify loess landforms using an object-based image analysis (OBIA) method and use this classification to describe the spatial variability of loess landforms. Quantitative indicators are used to drive the spatial variability analysis of loess landforms and explain their spatio-temporal evolution. Moreover, the hypsometric integral (HI) and topographic interpolation are employed to investigate soil erosion and development patterns of loess landscape. Results show that the OBIA method classified loess landforms to an accuracy of 88.7%. The derived metrics in terms of the area, slope and complexity of landform shape allow the determination of the spatial structure of the loess landscapes. The HI value of the entire basin is 0.486, representing the mature stage of landform development, with relatively severe surface erosion. Correlation analysis of HI values and related indicators in the sub-basins shows that HI is poorly correlated with the area proportion of loess landform types and the total erosion volume in the basin but shows a relatively strong correlation with the volume of erosion per unit area.

Keywords: Loess landform variability, hypsometric integral, object-based image analysis, landscape pattern indices, Chinese Loess Plateau

1 Introduction

Loess landscapes evolve due to the coupled effects of wind and water erosion (Xiong et al., 2014). In the Chinese Loess Plateau, these landscapes have attracted widespread attention, and numerous studies have been devoted to exploring their morphology, morphological change, and formative processes (Eger et al., 2012; Zhu et al., 2018; Feng et al., 2020; Li et al., 2020a; Guan et al., 2021; Hu et al., 2021). Less attention has been given to the spatial patterns of loess landforms over large spatial extents and how they can be used to infer loess landscape development through time based on the quantification of their spatial variability (Irvin et al., 1997; MacMillan et al., 2000; Wu et al., 2018; Yuan et al., 2020; Wei et al., 2021a). Typical loess landforms are composed of four elements: loess tablelands, loess ridges, loess hills, and loess gullies. Through a complicated combination of spatial distribution, area structure, topographic factors and environmental conditions, different loess landform elements shape the diverse loess landscapes, and these different landform expressions represent the spatial variability of the loess landforms (Tang et al., 2015; Xiong and Tang, 2019). Previous studies have proved that gully erosion is an essential contributor to shaping the diverse loess landform patterns (Wang et al., 2021; Liu et al., 2022b). Differential gully erosion in space not only changes the relative importance of these four elements but may change their shapes. The differences in the shape and spatial distribution of the four landform types are worth highlighting in spatial variability. This variability is recognized as specific manifestations of the different stages of loess landform development (Li et al., 2020a). Numerous methods and theories have now been proposed to explain the development of these stages (Stevens et al., 2013; Huang et al., 2019; Liu et al., 2020). They have contributed to a broader understanding of loess landform formation and evolution mechanisms. However, in relation to the Chinese Loess Plateau, such studies have tended to take a holistic perspective for the entire Chinese Loess Plateau, and exploration of spatial differences in loess landforms has primarily concentrated on certain loess landform types (e.g., loess tableland) rather than spatial variation in the relative importance and shape of different landform types. The analysis of spatial variability dictates that a large spatial extent is necessary, given that complete landform types and sufficient samples of landform entities are needed. Moreover, a large spatial extent may provide a broader perspective on the developmental modes and evolutionary processes of loess landscapes. This aspect is the focus of this study.

Early descriptions of loess landform variability were artistic (e.g., in paintings), highly visual, but not quantitative (Xiong et al., 2018; Cheng et al., 2020). With the benefit of rapid developments in remote surveying methods (e.g., unmanned aerial vehicle, lidar and InSAR), high precision topographic data has become more accessible and has facilitated more quantitative approaches (Lane et al., 1993; Hu et al., 2020; He et al., 2021; Xiong et al., 2021). Amongst them is the automated classification of loess landforms based on the analysis of imagery and/or digital elevation data by using either pixel-based (e.g. Dai et al., 2020) or object-based (e.g. Ding et al., 2021) approaches. Previous research found that pixel-based methods are sensitive to the land cover type and atmospheric conditions (Dingle and King, 2011; Chen et al., 2018; Jiang et al., 2021); and Object-based image analysis (OBIA) approaches have been proven to be effective over large areas (Shruthi et al., 2015; Liu et al., 2022a).

Classification is the precursor to describing and explaining the distribution of loess landform types. Descriptive indicators may be topographic factors or the shapes of two-dimensional morphological features. Topographic indicators focus on terrain derivatives, and more than 100 have been described to date for loess landform description (Tang et al., 2008). Two-dimensional morphological indicators do not necessarily need altitudinal data and focus more on shapes. Thus, they can be used when terrain data (i.e., elevation data) are unavailable.

One development of morphological indicators adopts a macro-perspective using landscape pattern indices more commonly used in landscape ecology. Landscape pattern is quantified in terms of structural composition and spatial configuration (Tischendorf, 2001; Li and Wu, 2004; Wei et al., 2021b). Landscape pattern indices were firstly applied to ecology-related research in the 1980s (Krummel et al., 1987) and have since been gradually expanded to a broader range of fields with the development of dedicated calculation software (Neel et al., 2004; Buyantuyev and Wu, 2007; Hassett et al., 2012;).

The advantage of landscape pattern indices is that they can distinguish differences in the characteristics of the study target at multiple scales in terms of patches, classes and landscape in parallel to the quantification of common morphological characteristics (Wang et al., 2014). Furthermore, indices are available to express the spatial distribution, clustering, and diversity of investigated objects (McGarigal, 2001). Convenient calculation and a wealth of optional indices make landscape pattern indices attractive to researchers.

To investigate the development of loess landforms, the assessment of the stages of loess landforms evolution is the foundation, represented by the extent of surface erosion. The latter can be measured by comparing topographic changes for different periods and inferring the erosion rates from mass conservation (Antoniazza et al., 2019; Dai et al., 2021). In this study, the loess landform development is inferred from the hypsometric integral (HI), a widely used indicator in geomorphology, hydrology and active tectonics studies (Lifton and Chase, 1992; Ohmori, 1993; Willgoose and Hancock, 1998; Zhang et al., 2020). The HI indicator describes the relative proportion of the basin area that lies at or above a given elevation relative to the total basin topography, and the shape of the hypsometric curve can be used to infer the stage of landform development (Strahler, 1952). This index was firstly introduced by Strahler (1952) and later extended to a broader range of fields. The development of computational platforms and DEM data has reduced the calculation difficulty of HI, which makes it more widely applicable and practicable (Luo, 1998).

Building on an OBIA classification of loess landforms in the Luohe River Basin of the Chinese Loess Plateau, this study uses a system of descriptive indicators of loess landform development to quantify the large-scale spatial variability in loess landforms. This analysis is then used to understand the development of loess landscapes through the progressive process of gully erosion. The specific objectives of this study were to (1) assess the performance of the OBIA method in the classification of large-scale loess landforms, (2) construct a quantitative indicator system for describing loess landform variability in space and (3) analyze the evolution of loess landforms within the case study as compared with existing theories of loess landform development.

2 Material and methods

2.1 Study area

The Luohe River Basin is located at the hinterland of the Chinese Loess Plateau (107°32′-110°06′E, 34°54′-37°19′N), with an area of approximately 3.68 $\times 10^3$ km^2 (Fig. 1). The overall elevation is high in the northwest (maximum altitude of 1741 m) and low in the southeast (minimum altitude of 410 m). The basin has a continental monsoon climate, with an average annual rainfall between 510 and 540 mm concentrated in July to September. Intense rainfall leads to soil loss in this basin and affects approximately 64% of the total area of the watershed (Wu et al., 2014). The study area has typical loess landform features, and the loess landform patterns of the basin show significant regional variation. The main landform types of the basin from top to bottom are the hilly-gullied loess region upstream, then the plateau gully region, and finally the plain terrace region downstream, with relatively flat topography. According to the landform type map of the Chinese Loess Plateau, the landform types in the study area include loess tablelands, residual tablelands, gullies, and low bedrock hills (Guo et al., 2015). Owing to the visible differences in the intensity of gully erosion, it is an ideal sample area for studying the loess landform variability and its spatial distribution. For computational reasons and because it showed the full range of loess landform types, the downstream area of the Luohe River Basin was selected as the study area (Fig. 1b). The downstream area of Luohe River Basin is divided into several sub-basins, and the actual analysis area is slightly smaller than the downstream of the Luohe River Basin.

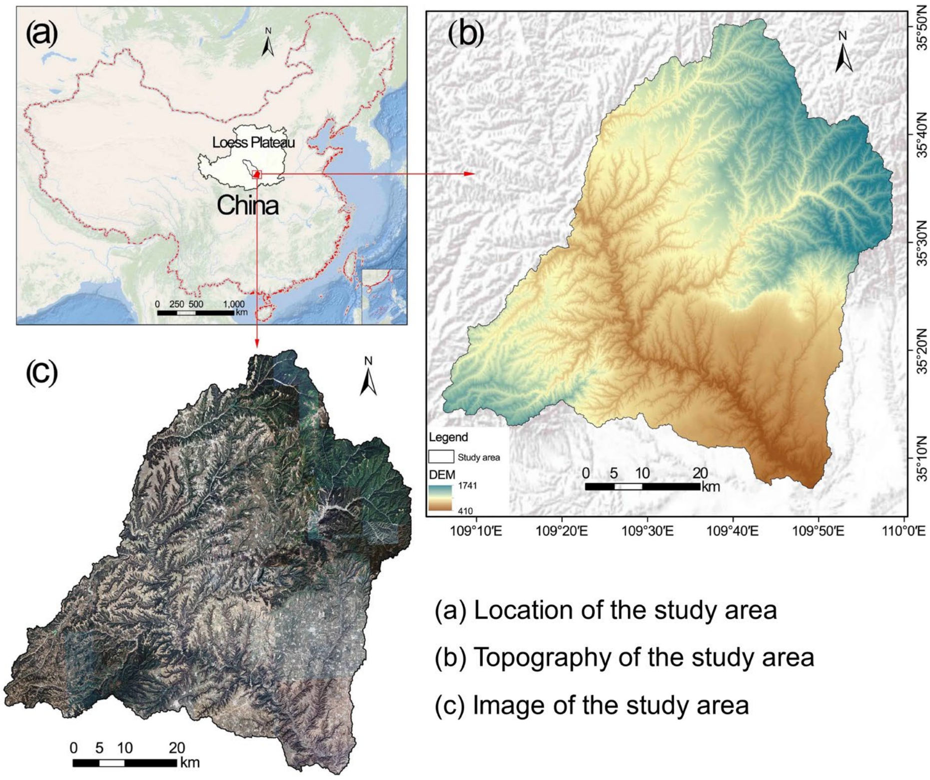

Fig. 1. Location of the study area (Fig. 1a), the associated Digital Elevation Model (DEM) (Fig. 1b) and the Planet Explorer image of the study area (Fig. 1c)

2.2 Data sources

The data used in the research are topographical, hydrological, and image-based. The topographical data were derived from the NASADEM released by the National Aeronautics and Space Administration (NASA) in 2020 with a spatial resolution of 1 arc second, considered the highest-quality freely-available product with global coverage (Crippen et al., 2016). High-resolution remote sensing images were used to produce higher density spectral and texture information. The imagery of 5 m resolution downloaded from Planet Explorer (https://www.planet.com/explorer/) was used. The image data were mainly captured between January and April in 2021. During this period, less vegetation cover is present on the surface, and the boundaries of loess morphology objects are more obvious, which aids image segmentation and classification. Terrain factors (slope, aspect, curvature and hill shade) and vector river data were also used as auxiliary layers to support the image segmentation process. The terrain factors used were calculated using the 1 arc second resolution DEM at approximately 30 m resolution and vector river data provided by the Upper and Middle Yellow River Reaches Administration.

2.3 Methods

2.3.1 Loess landform interpretation based on the OBIA method

The OBIA method was adopted to classify the loess landform types of the study area. The overall landform classification flowchart is shown in Fig. 2. The two most important steps in the classification process are the segmentation of multiple layers and the selection of classification features (Yan et al., 2006). In this research, the segmentation was conducted in the eCognition Developer 9.0 (Trimble) software using multiresolution segmentation (MRS) (Johnson and Jozdani, 2018). MRS is a bottom-up region merging technology starting from a pixel object (Nikfar et al., 2012; Liu et al., 2017). Adjacent image objects are merged to meet the defined minimum growth criteria for heterogeneity; otherwise, the merging process stops. The image object generated after the segmentation process is the smallest unit for further image interpretation. Multiple input layers are necessary to provide as much information as possible to distinguish segmented objects.

Thus, DEM data, derived terrain factor layers, remote sensing images, and vector river data are used in classification experiments.

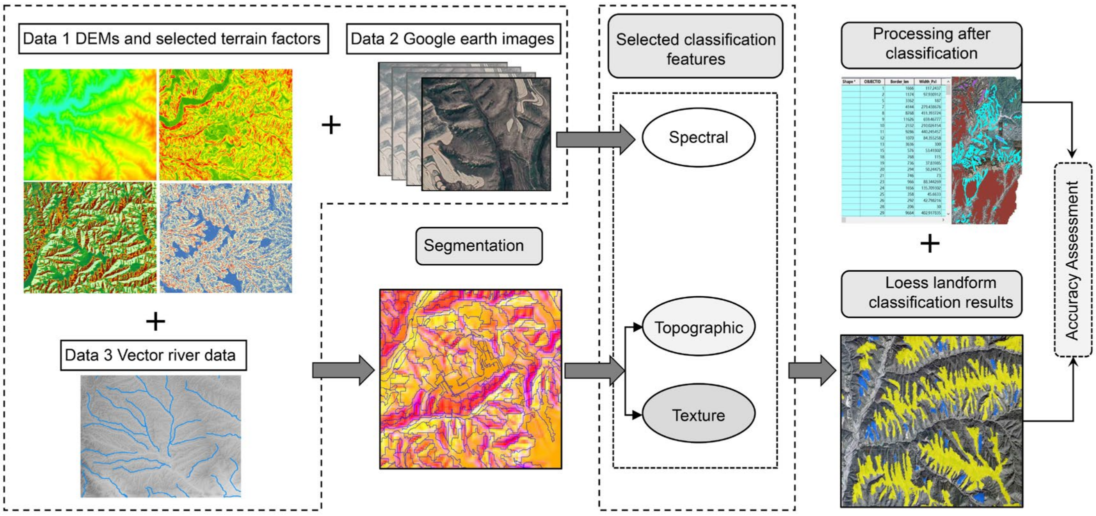

Fig. 2. Flow chart of loess landform classification process

In MRS, the main parameters that control image segmentation are the weight given to different input layers, the segmentation scale parameter, the shape weight, and the compactness weight. Firstly, considering that topographical and spectral features are important factors in the classification process, the input layers were equally weighted in the segmentation. The shape factor and smoothness were set to 0.3 and 0.5, respectively. Secondly, the scale parameter estimation (ESP) tool was adopted to determine the optimal segmentation scale, developed by Drăguţ et al. (2010) to identify optimal scale parameters automatically. ESP calculates the local variance of a certain scale as the average standard deviation of all image objects under its scale and selects the optimal segmentation scale according to the local variance curve and its scale parameters (Drăguţ et al., 2011). When the local variance reaches a maximum, and the rate of change up to a peak, the spatial heterogeneity of all image objects in this scale is the largest. By analyzing and comparing different extremum points, the optimal scale of image classification is ultimately determined

(Drăguţ et al., 2010). After several tests and fine-tuning, the final segmentation scale was set to 45.

The classification of the segmented objects is conducted using a decision tree. By calculating and counting spectral, geometric, and terrain characteristics of image objects, the spatial and attribute characteristics of different geomorphic types are statistically analyzed, and the features with significant differences are selected to establish the decision tree (Benz et al., 2004). Firstly, the image is divided into two parts: gully and non-gully areas. The gully is the most easily distinguished part of the loess landform because of its low elevation and steep slope. In the meantime, the rich vegetation coverage causes low brightness values in the image, and this causes flatter gully bottoms also to be classified as gully. According to these characteristics, the main body of the gully can be extracted. Non-gully areas are divided into loess tableland, loess ridge, and loess hill according to indicators such as area, slope, and length-width ratio (Fig. 3). In this process, manual visual interpretation is also applied for auxiliary landform classification in areas with poor image feature discrimination to obtain higher classification accuracy.

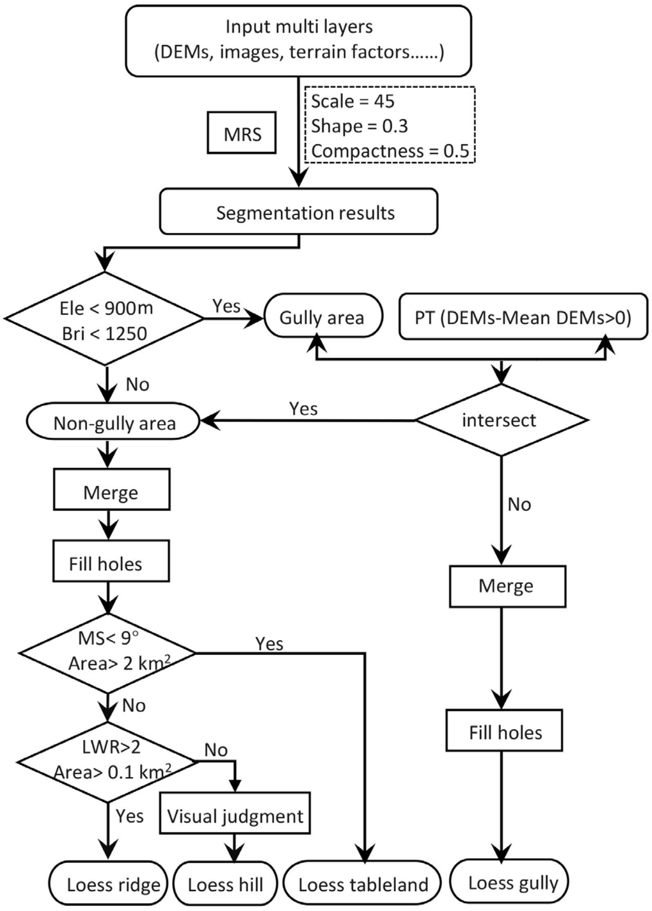

Fig. 3. Decision tree for loess landform classification

Note: Elevation (Ele), Brightness (Bri), Positive terrain (PT), Mean slope (MS), Length–width ratio (LWR).

2.2.2 Hypsometric integral

Three main methods are currently available to calculate the HI value: the integral curve method (Luo, 1998), the volume ratio method (Meerkerk et al., 2009), and the elevation–relief ratio method (Pike and Wilson, 1971). In this study, the integral curve method is applied. This method uses the relative height ratio (h/H) in the target area as the vertical axis and the relative area ratio (a/A) as the horizontal axis to draw the integral of the area elevation integral curve (Strahler curve) in [0,1] (Pérez-Peña et al., 2009). The smaller value of HI means that the erosion of the surface is more severe. The formula is as follows:

$$\mathrm{HI}=\int_1^0 \mathrm{f}(x)dx \quad (1)$$

The criteria for grading HI values are as follows: areas with HI above 0.6 are in the 'youth' stage, areas with HI between 0.35 and 0.6 are in the 'mature' stage, whereas areas with HI below 0.35 are in the 'old' stage of landscape development (Strahler, 1952).

2.2.3 Erosion estimation

The volume of surface material loss is a representative indicator of the intensity of surface erosion. This research estimated the volume of erosion associated with loess gullying by subtracting the current DEM from an interpolated initial surface, estimated as the original topography prior to the onset of loess gully erosion. The initial surface is theoretically based on the assumption that the current existing loess tableland represents the original ground of the basin before the loess gully starts (Li and Lu, 1990). The extracted loess tablelands were regarded as the remaining initial ground surface. The loess tablelands were transformed into data points, and then spline interpolation was used to interpolate an initial ground surface. The spline interpolation applies a mathematical function to estimate values that minimize the overall surface curvature and is appropriate for interpolation to generate smooth continuous surfaces such as elevations (Franke, 1982; Yang et al., 2015). The volume of material that should have been lost from the basin can be estimated by counting positive and negative differences of DEMs by superimposing the current DEM and the interpolated DEM. The quality of the interpolation results is evaluated using the root mean square error (RMSE), which is calculated as follows:

$$RMSE=\sqrt{\frac{1}{N}\sum_{k=1}^{N}(Z_i-z_i)^2} \quad (2)$$

Where N is the total number of validation points, Z_i is the real elevation of the validation point, and z_i is the interpolated elevation of the validation point. The lower value of RMSE implies that the interpolation is better and the accuracy of the result is higher.

2.2.4 Landscape pattern index

Various landscape pattern indices are available to quantify loess landform types. However, some of them have similar meanings and are strongly correlated (O'Neill et al., 1988; Wu et al., 2012; Rahimi et al., 2021). To ensure the selected indices are comprehensive and non-redundant, ten indices were employed to quantify the characteristics and spatial distribution of loess landform types based on four themes; morphological, topographic, spatial distribution, and quantitative structural. They are shown, along with their calculation methods, in Table 1 (Wu et al., 2017). Fragstats 4.2 software was used to calculate these landscape pattern indices, and a more detailed introduction of these indices can be found in the documents for Fragstats (McGarigal, 1995).

Table 1 Selected landscape index and its description

index	Formulation	Formula description
Mean patch size (MPS)	$MPS=\frac{A_i}{N_i}10^{-6}$ *A_i* is the total area of loess landform *i*, *N_i is* the total number of patches of landform type *i*.	This indicator can reflect the average patch area size of landform types (unit: km^2).
Mean patch perimeter (MPP)	$MPP=\frac{P_i}{N_i}10^{-3}$ *P_i* is the total perimeter of loess landform *i*.	MPP reflects the mean patch perimeter of landform types
Mean elevation (ME)	Calculated in ArcGIS platform	ME and MS reflect the topographical features of the patch
Mean slope (MS)	Calculated in ArcGIS platform	
Length–width ratio (LWR)	$LWR=\frac{1}{n}\sum_{i=1}^{n}\frac{l_i}{w_i}$ *l_i* is the length of patch i, *w_i* is the width of patch i, *n* is the total number of patch *i*.	LWR reflects the shape features of patches. The closer the value is to 1, the more similar it is to square.

Circularity index (CI)	$CI = p_i / 2\sqrt{\pi a_i}$ p_i is the edge length of patch *i*, a_i is the area of patch *i*.	CI represents the similarity between patch shape and circle. The closer the value is to 1, the closer the patch is to circle.
Area weighted mean shape index (AWMSI)	$AWMSI = \sum_{i=1}^{n}[(\frac{0.25 p_i}{\sqrt{a_i}})(\frac{a_i}{A_i})]$ *n* is the total number of patches of a certain loess landform type.	AWMSI reflects the complexity of the patch, the larger the value, the more irregular the shape
Largest patch index (LPI)	$LPI = \frac{Max(a_1, a_2, ...a_n)}{A}(100)$ A is the total area of the study area.	LPI reflects the dominant type in the loess landform landscape.
Mean nearest neighbor (MNN)	$MNN = \frac{\sum_{i=1}^{n} d_{ij}}{n}$ d_{ij} is the distance between patch *i* and its nearest patch *j*.	MNN calculates the spatial distance between patches in loess landform type and reflects patch dispersion.
Aggregation index (AI)	$AI = [1+\sum_{i=1}^{m}\sum_{j=1}^{n}\frac{P_{ij}\ln(P_{ij})}{2\ln(m)}]*100$ *m* is the total number of landform types, P_{ij} is the probability that two adjacent grid cells randomly selected belong to loess landform types *i* and *j*.	AI is a measure of the aggregation of the same type of patches.

2.2.5 Subdivision of basins for analysis

To analyze the correlation between loess landform variability and landform evolution, the study area was divided into several sub-basins. The Soil and Water Assessment Tool (SWAT) model was used to divide the sub-basins for allowing within study area comparisons. The SWAT model was developed by the USDA Agricultural Research Service to simulate land management processes and rainfall-runoff processes for a more detailed spatial scale by dividing the watershed into smaller sub-watersheds (Arnold et al., 1998; Zheng et al., 2010). On the basis of the topographic information provided by the DEM data, the study area was divided into 10 sub-basins, with areas ranging from 122 km^2 to 855 km^2 (the threshold for the sub-basin area was set at 150 km^2, but one basin with an area of 122 km^2 was included to guarantee that the full study area was included.)

3 Results

3.1 Classification results for loess landform types

Fig. 4 presents the classification results of loess landforms in the study area. The classification results clearly demonstrate the differences in the spatial distribution of the loess landscape. By area, the classification suggested that the main landform types of the study area are loess tableland and loess gully, and the area of loess ridge and loess hill is relatively small. The loess tablelands are distributed on both sides of the Luohe River, the loess ridges are mainly distributed in the east and west regions of the study, and the loess hills are scattered across the study area.

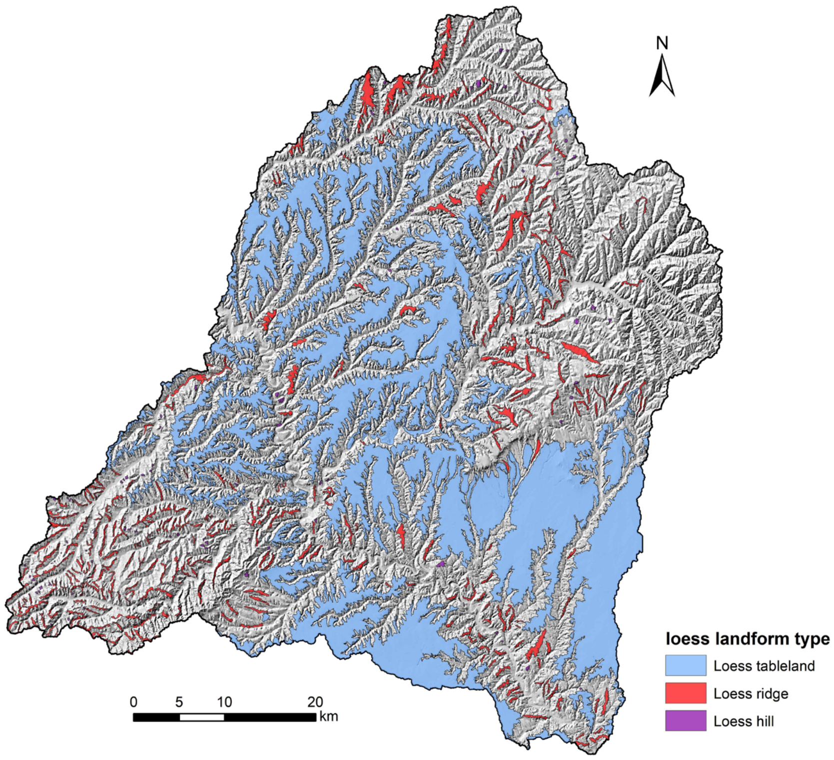

Fig. 4. The classification results of loess landforms in the downstream of the Luohe River Basin

A total of 62 loess tablelands, 330 loess ridges, and 121 loess hills were identified in the study area. The accuracy of the classification results was verified for 300 randomly selected points in the study area, and the selection of the verification points was stratified to guarantee a certain number of points for each loess landform type. The resultant confusion matrix is shown in Table 2. The number of total points that are correctly classified after verifying is 266, the overall classification accuracy is 88.7%, and the kappa coefficient is 0.801. Therefore, the OBIA method adopted in this study achieves an excellent classification performance. Especially in the loess tableland, the most satisfactory classification was performed with a commission error of 5.06%. However, the classification of the loess hill and loess gully is poorly represented, with 25% and 22% commission errors, respectively. The points that failed the verification are mainly found in the loess gullies. The main reason may be that the large-area terraces built in the study area changed the topography of the gullies and simultaneously changed the characteristic spectral values of the gullies on the image resulting in poor classification accuracy of the loess gullies.

Table 2 Confusion matrix and accuracy statistics of extraction results.

	Tableland	Ridge	Hill	Gully	Prod. Ac	User. Ac	Com. Er
Tableland	169	4	0	5	94.94%	96.02%	5.06%
Ridge	1	21	0	3	84%	53.85%	16%
Hill	0	2	12	4	75%	100%	25%
Gully	6	12	0	64	78.05%	84.21%	21.95%

Note: Prod. Ac, Producer accuracy; User. Ac, User accuracy; Com. Er, commission error.

3.2 Quantitative analysis of loess landform development degree

The loess landform classification results suggest that the spatial distribution of different loess landforms is variable, reflecting the differences in the development stages of different regions. The area proportions and erosion of the loess landforms in each sub-basin were counted to provide a more detailed analysis of the loess landform variability of the sub-basins. The simulated initial surface for the erosion estimation was generated by interpolation based on loess tablelands with an RMSE of ±3.14 m. Although the interpolated results have limited precision, an approximate estimate of the amount of material eroded from the surface is provided. Table 3 shows the main loess landform features in each sub-basin, including the area proportion of different loess landform types, the total area of each sub-basin (TA), eroded volume (EV), and erosion volume per unit area (UEV).

It is evident that the composition of the loess landform varies considerably between sub-basins. Loess gullies are the dominant landform type in all sub-basins, with the proportion of their area exceeding 50%, and in sub-basins 1, 4, 6, and 7 exceeding 80%. This finding indicates that the whole basin has been subjected to intense erosion, and the intersecting loess gullies fragment the surface. After the loess gullies, the dominant loess landform type in the basin is loess tableland, which is accompanied by a small number of loess ridges and loess hills. Amongst these sub-basins, 8, 9 and 10 have the highest proportion of loess tablelands and contain most of the loess tablelands in the study area (Fig. 5). This spatial distribution is due to the marked spatial variation in the loess landscape of the study area. The western part of the basin belongs to the long ridge and gully region, the surface of which is dominated by loess ridges and loess hills. The eastern part of the basin is a low mountain region, where only a few loess ridges and loess hills can be found. The geographical conditions of the two parts of the region make it challenging to preserve the large areas of loess tablelands. The loess tablelands are mainly distributed along both sides of the Luohe River in the central part of the study area, and the further downstream the area, the closer it is to the Guanzhong Plain and the flatter the ground is. Thus, a large area of loess tablelands is formed in sub-basins 8, 9 and10.

Table 3 statistics of loess landform features in the sub-basins

sub-basin	tableland	ridge	hill	gully	TA	EV	UEV	HI
1	10.39%	7.02%	0.42%	82.17%	320.68	11.89	0.0371	0.457
2	44.57%	0.75%	0.05%	54.62%	202.61	7.14	0.0353	0.507
3	35.65%	1.72%	0.11%	62.53%	246.49	10.43	0.0423	0.464
4	11.64%	7.16%	0.71%	80.48%	188.71	8.51	0.0451	0.445
5	44.70%	1.30%	0.18%	53.81%	271.27	11.76	0.0433	0.468
6	6.14%	8.16%	0.29%	85.41%	340.33	10.69	0.0314	0.511
7	11.68%	3.65%	0.14%	84.53%	854.82	25.63	0.0300	0.593
8	45.48%	2.49%	0.10%	51.94%	772.68	45.17	0.0585	0.354
9	43.33%	2.67%	0.14%	53.87%	255.72	13.83	0.0541	0.396
10	44.05%	3.60%	0.03%	52.32%	122.27	3.32	0.0272	0.572

Note: TA, total area (km^2); EV, eroded volume (km^3); UEV, unit eroded volume (km^3/km^2).

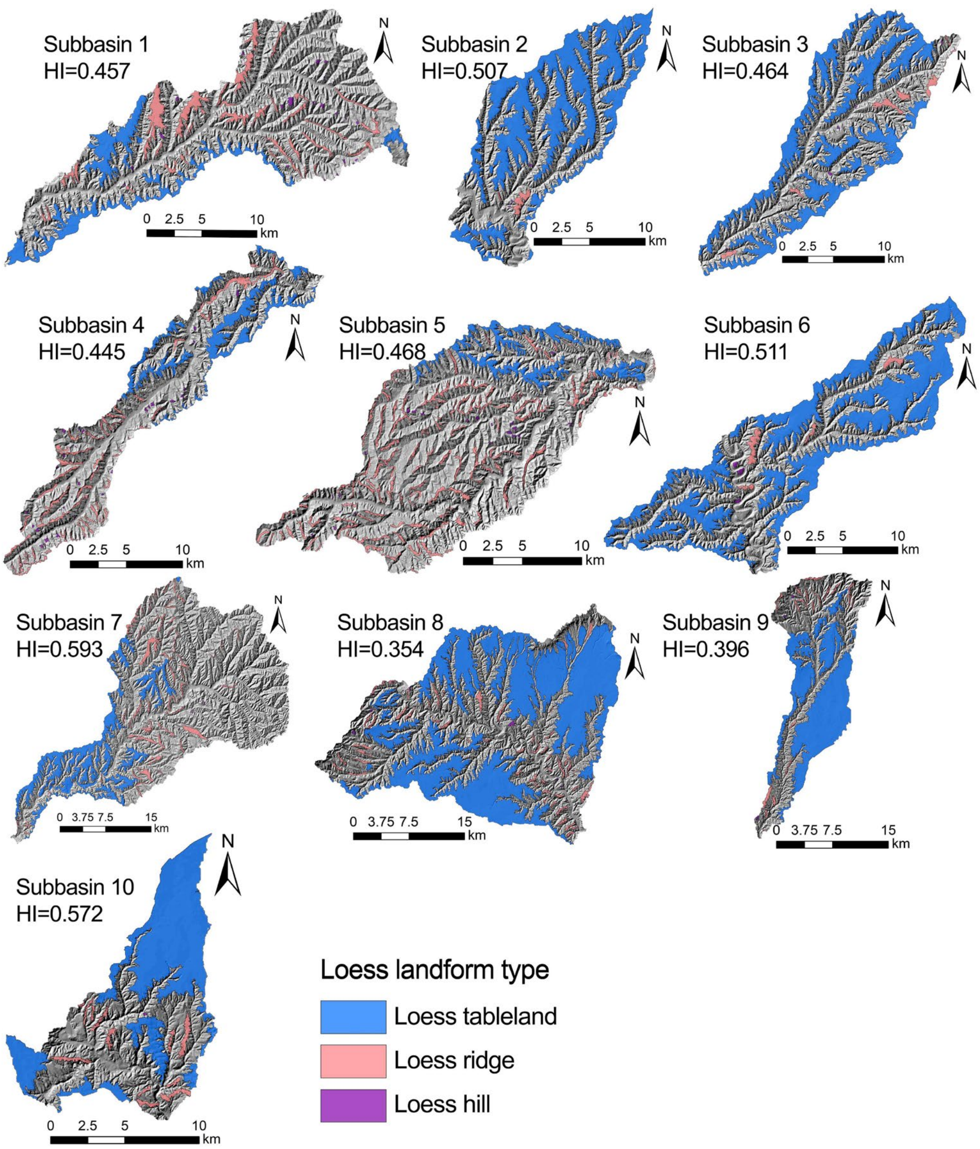

Fig. 5. Spatial distribution of loess landform types in the sub-basins

The study area HI values of each of the ten sub-basins were calculated (Fig. 6) to assess the correlation between the developmental stages and the spatial variability of the loess landforms. The HI value for the whole basin is 0.486, which implies that the study area has transitioned from the youth stage of landform development to the mature stage. The HI values for the sub-basins range from 0.354 to 0.593, with a wide range of variation and spatial variability. The HI values of the sub-basins have a general decreasing trend from north to south (direction of the Luohe River flow), which means that the degree of surface erosion in this direction is gradually increasing. Sub-basins 6 and 7, located on both sides of the Luohe River, have higher HI values than those in the central region. This finding implies that erosion is more developed closer to the Luohe River. Sub-basins 8 and 9, which are downstream of the basin, have the lowest HI values of 0.345 and 0.396, respectively. Therefore, the loess landform development is nearing its most mature. Theoretically, the HI values for loess tableland areas should be greater than those for loess ridge-hill areas, due to loess tableland being the primary form of early landform development (Guo et al., 2015). However, in the present study, the opposite results are found. The HI values in the loess tableland area (sub-basins 8 and 9) are smaller than those in the ridge-hill areas (sub-basins 1, 4, 6 and 7). This phenomenon may be because sub-basins 8 and 9 are situated downstream of the Luohe River, with the accumulated river runoff having caused significant scour and encouraged more intense gullying. Meanwhile, the loess tableland area is the primary inhabited zone, especially since the launch of the "population transfer to tableland", where the population density has now reached 180 persons/km^2 (Guo et al., 2015; Zhang et al., 2016; Lu et al., 2017). Cultivation and human activities have enhanced the erosion intensity in the loess tableland. Some studies have shown that the modern erosion rate in the loess plateau is four times the average since the Holocene geological period (He et al., 2004).

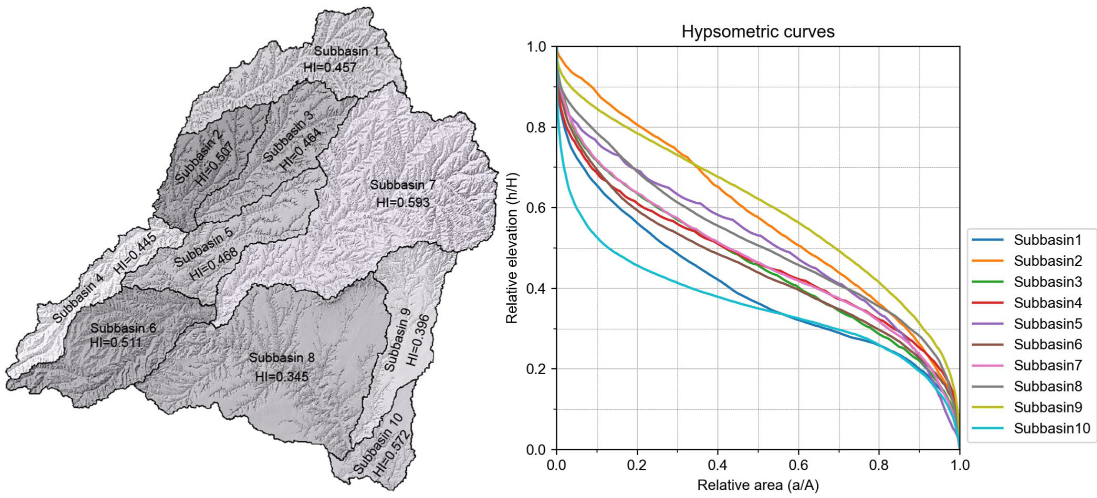

Fig. 6. Spatial distribution of sub-basins and their HI curves

Some studies have emphasized that a correlation exists between the stage of landform development and loess landform variability (Zhang et al., 2015; Li et al., 2019). Thus, we compared the HI values with sub-basin parameters (Fig. 7). The results show no obvious relationship between the proportion of different loess landform types by area and the HI values, as well as with the total erosion volume. Nevertheless, a strong linear relationship is observed with the erosion volume per unit area (UEV); the coefficient of determination (R^2) between UEV and HI is 0.898. The explanation for this phenomenon is that HI reflects the stage of landform development, and its value reflects the proportion of the original material left on the surface (Strahler, 1952). Loess gullies are directly related to surface erosion. Thus, theoretically, they should show a certain correlation with HI values, but this relationship is not observed in this study. The reason is that the factors affecting the volume of gully erosion include gully area and depth. Thus, considering only the gully area fails to fully reflect the intensity of gully erosion. Correspondingly, the gully area shows no strong correlation with HI values. The total erosion volume in a basin is controlled by the surface erosion intensity, as well as the size of the basin. In the meantime, the UEV can quantify the surface erosion intensity. This finding explains the high correlation between UEV and HI values, but not the total erosion volume.

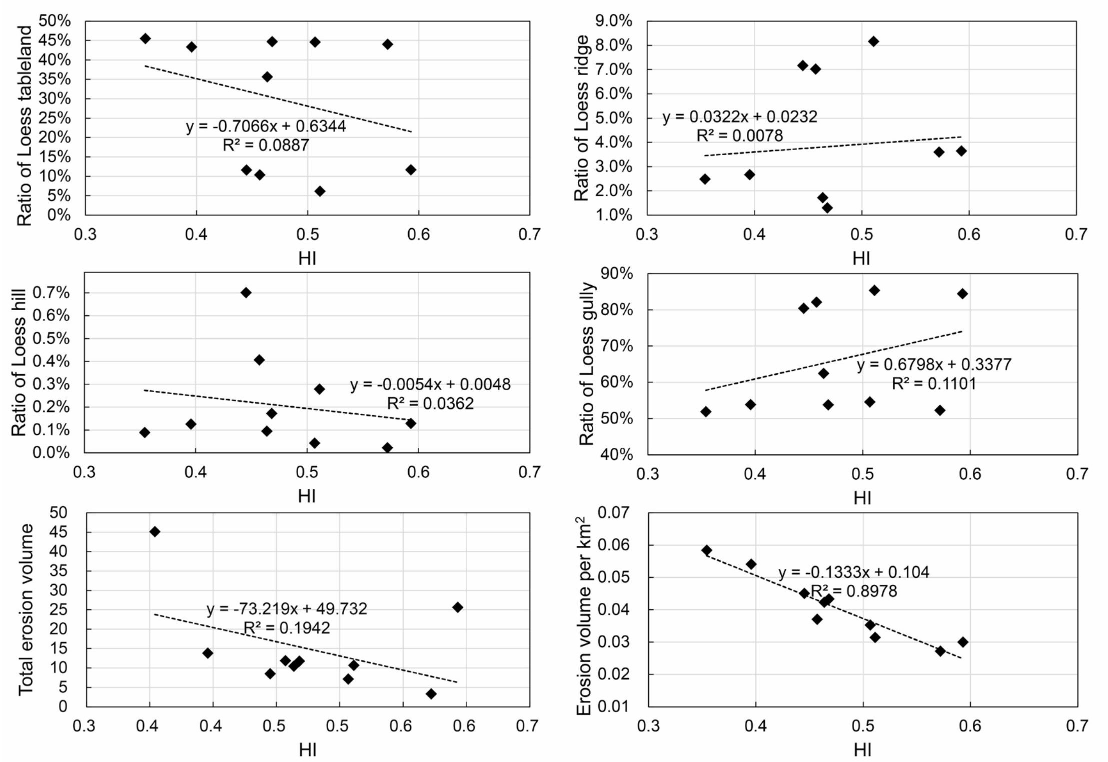

Fig. 7. Relationships and changes in HI values with loess landform features

3.3 Analysis of landform patterns

The landform pattern indicators suggest a significant difference between different loess landform types (Fig. 8). The most notable difference lies in the MPS and MPP indices. The average patch size of the loess tableland is 21.5 km^2, which is much larger than that of the loess ridge (0.42 km^2) and the loess hill (0.06 km^2) (Fig. 8a). For the loess tableland, the larger patch area is accompanied by a longer patch perimeter (Fig. 8b). In terms of topographical characteristics, the loess tableland has a smoother terrain with an average slope of 8.41° and the lowest average elevation. The average elevation and slope of the loess ridge and the loess hill are significantly greater than that of the loess tableland, but the topographical difference between the two types is not obvious (Fig. 8c; 8d).

The three types of loess landforms have similarly significant differences in morphological indicators. The LWR index reflects the degree of patch extension. For this indicator, the order of the three types is loess ridge, loess tableland, and loess hill; this order indicates that the shape of the loess ridge is narrower and longer (Fig. 8e). In contrast to the LWR, the CI index reflects the similarity between the patch shape and the circle. As observed, the shape of the loess hill is closest to a circle, followed by the loess tableland and loess ridge (Fig. 8f). The AWMSI index reflects the complexity of the shape of the patch. The larger value implies that the shape of the patch is more complex. The AWMSI value of the loess tableland is 8.62, which is much larger than the loess ridge (3.37) and the loess hill (1.62), indicating the shape of the loess tableland is the most complex; the shapes of the loess ridge and loess hill are relatively simple (Fig. 8g). The main reason is that the loess residual tableland dominates the loess tableland in the study area. The gullies eroded their shape from multiple cut-in points and developed into a network with different levels of gullies inside, forming irregular loess residual tableland. The loess ridge and loess hill are small in area and perimeter and simple in shape. As a result, the AWMSI index is low. By contrast, the loess ridge and loess hill are independent elements separated by gullies with simple shapes. Accordingly, the AWMSI index is lower.

The LPI index reflects the proportion of the largest patch to the total study area and is an indicator that measures the dominant landform type. The LPI index of the loess tableland is much larger than that of the loess ridge and the loess hill, indicating that the loess tableland is in a dominant position in the study area (Fig. 8h). MNN and AI indices reflect the connectivity and aggregation degree between landform patches, that is, the spatial distance between patches and the concentration degree of patch distribution. In general, the spatial distance between patches is smaller and the connectivity is higher when the patch distribution is more aggregated. The MNN and AI indices of loess tablelands are the largest, followed by those of the loess ridge and loess hill landforms (Fig. 8i; 8j). The differences between loess ridge and hill landforms are not significant. The loess tablelands in the study area originally belonged to the Luochuan tableland, which is a large loess tableland. Given that the erosion of the gullies is a gradual process, the spatial distance between the loess tablelands cut by the gullies is small, and the distribution is relatively dense. However, the locations of loess ridge and loess hill landforms are randomly distributed accompanied by a discrete spatial distribution, and the aggregation degree is low, which leads to the low values of the MNN and AI indices.

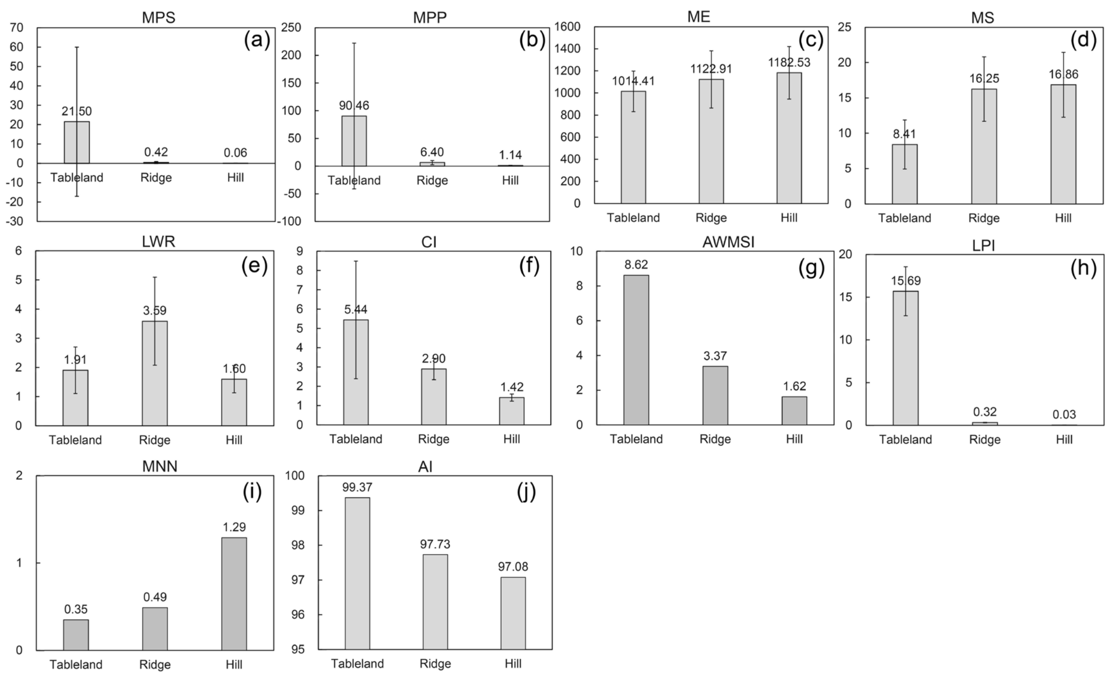

Fig. 8. Quantitative indices of loess landform types. (a) mean patch size, (b) mean patch perimeter, (c) mean elevation, (d) mean slope, (e) length-width ratio, (f) circularity index, (g) area weighted mean shape index, (h) largest patch index, (i) mean nearest neighbor and (j) aggregation index. Standard deviations are shown for 8a through 8f, and 8h.

4 Discussion

4.1 Analysis of evolution process of loess landform

It is generally accepted that the evolution of loess landforms is gradual with four stages, from loess tableland to residual tableland, to loess ridge, and ultimately to an isolated loess hill (Zhao and Cheng, 2014). Some scholars have emphasized that not all loess landform systems follow this evolution model, special cases exist such as the direct evolution of marginal areas of loess tableland into loess hill. Nevertheless, a consensus exists: the evolutionary tendency of the loess tableland to the loess hill is a nearly universal phenomenon (Tang et al., 2015). During the main phase of gully development, the material loss from individual loess landform objects gradually increases as surface erosion progressively intensifies. Here we show that this evolution is accompanied by changes in core quantitative indicators such as the shape and area of loess landforms (Fig. 8).

The analysis of quantitative indicators of loess landform patterns in the study area shows that the loess tableland area is usually relatively large. The terrain is gentle, with a slope of about 8°. However, in the edge zone of the loess tableland, the terrain is relatively steep, and it is susceptible to the influence of hydraulic erosion as loess gullies develop. The loess tableland is also the main region for human cultivation and habitation. Cultivated and residential lands are the main runoff and sediment source areas that contribute to soil erosion; thus, soil erosion processes are accelerated for loess tableland (Chen et al., 2008). This erosion process usually starts from the edge of the loess tableland and gradually erodes inwards. Under the action of long-term edge erosion, the loess tableland gradually develops and forms the loess residual tableland. A specific example is shown in Fig. 9a. Three loess residual tablelands originally belonged to a complete loess tableland. Several north-south oriented gullies eroded this area independently but these effects combined to divide the loess tableland into three residual tablelands. In the meantime, new gullies developed and continued to erode the loess residual tablelands.

The residual tablelands have smaller areas (by definition), more complex shapes, and longer perimeters than the original loess tableland. With the continuous advancement of the loess gullies, areas inside the loess residual tablelands are continuously eroded until the gullies are entirely cut through. The loess residual tableland is decomposed into long independent loess ridges. A specific example is shown in Fig. 9b. The three loess ridges and the loess residual tableland were originally a single loess tableland. The development of the loess gullies divided the three loess ridges to form independent loess landform objects. Given that the loess ridge is separated from the loess residual tableland, its area and perimeter are much smaller than those of the loess residual tableland, and its shape is relatively simple. In this case, the total area of the three loess ridges separated from the loess residual tableland is 4.0 km^2, accounting for only 14.4% of the loess residual tableland. The distribution of the parts cut through by the gullies is relatively random. Thus, the distribution of the loess ridges is relatively scattered, resulting in a low degree of physical connection between the loess ridges and a low degree of distribution aggregation.

As a result, the loess ridge's AWMSI, MNN and AI indices are significantly lower than those of the loess plateau (Fig. 8g; 8i; 8j).

The evolution from loess ridges to loess hills is relatively slow, mostly from short-wide ridges to irregular hills. Following Fig. 8e; 8f and 8h, differences between loess ridges and loess hills are small in topographic and spatial distribution characteristics but larger with regard to shape characteristics, such as the LWR, CI, and LPI indices. The crest of the loess ridge is relatively flat, but the slope is larger at the surrounding edges, which is more prone to erosion. The evolution of loess ridge to loess hill includes two kinds of change. One is that the edges of the short-wide loess ridges are eroded. Under the smoothing effect of the edge erosion, the shape of the loess ridge changes slightly and gradually forms a loess hill. The second occurs where gullies cut through the main part of the long-narrow loess ridge, and the separated loess landform object forms a loess hill. The specific case is shown in Fig. 9c. The loess hill shown in yellow has been completely separated from the loess ridge, forming an independent individual object with a smaller area and a more regular shape. This figure also shows the complete evolution process from the loess tableland to the loess ridge and then to the loess hill, in which the gully development and erosion play a dominant role.

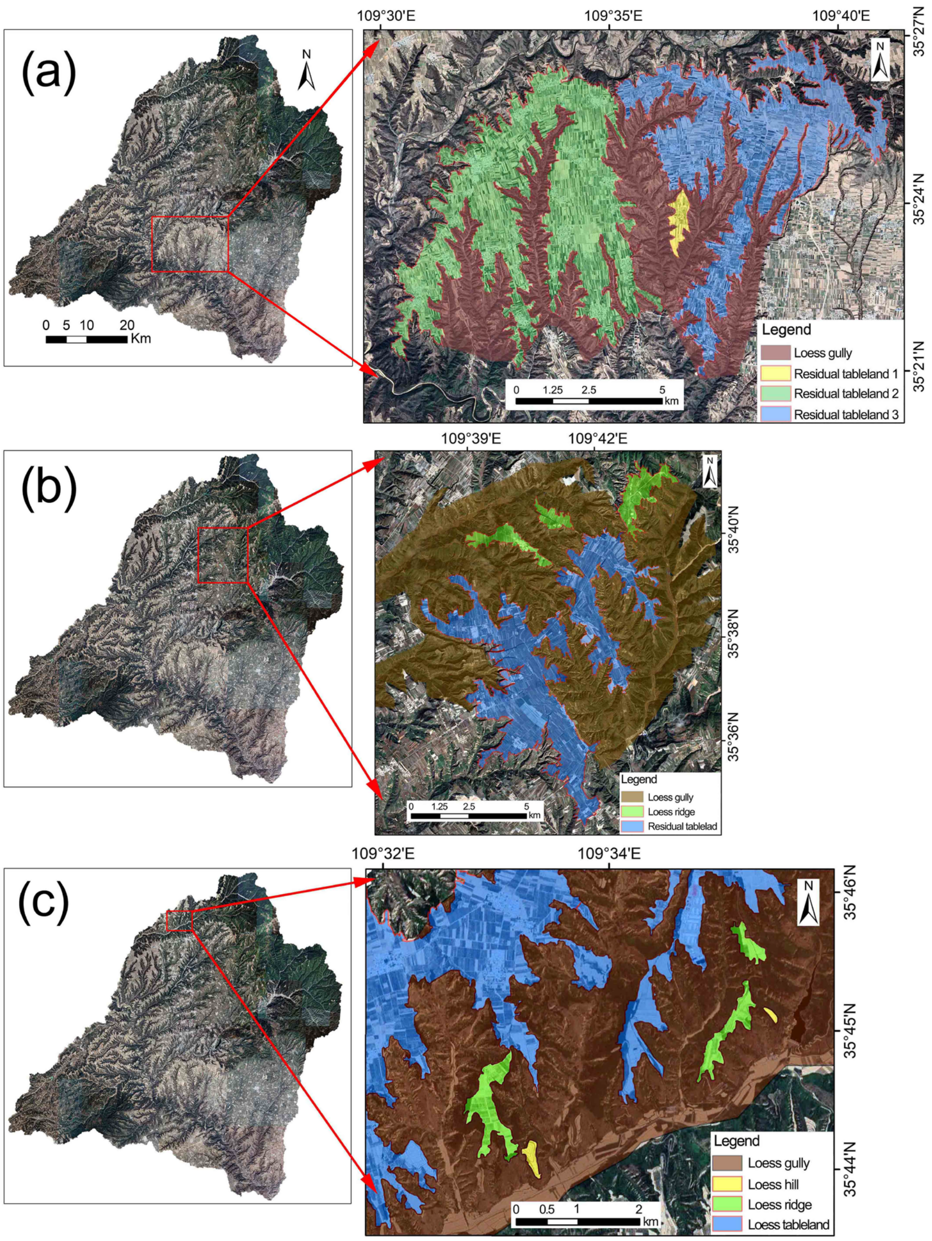

Fig. 9. Example diagram of development and evolution of loess landform types

4.2 Perspectives on the methodological approach

The gully interpretation method employed in this study utilizes OBIA combined with some visual interpretation, which is affected to a certain extent by the experience and knowledge of the interpreter. Although this method will be affected by subjective factors, it still has certain advantages in landform classification. Some scholars pointed out that the OBIA method is superior to the traditional pixel-based classification method because the analysis object has changed from a single pixel to a more meaningful geomorphological object (Aplin and Smith, 2011). In addition, some scholars use the machine learning method to recognize loess landforms. However, the potential of the machine learning method in large-scale image interpretation has not been fully explored (Ding et al., 2020; Li et al., 2020b; Li et al., 2022).

HI values are an essential parameter for understanding loess landform development, but limitations still exist. The prerequisite for applying the HI value is that the landform development is a completely closed system by default, and the evolution of the landform is entirely controlled by internal forces (Strahler, 1952). However, the development of loess landforms does not fully conform to this hypothesis, and its development is disturbed by various factors, including rainfall, land use, and anthropogenic activities (Wang et al., 2016; Zhou et al., 2021;). Some scholars have also developed other indicators to quantify the stage of landform development, such as entropy. Entropy is a concept that relates to thermodynamics and describes the state of an element. Ai (1987) found that entropy was also applicable to expressing the status of landform and proposed a method for calculating landform entropy (Ai, 1987). Following this calculation method, we also calculated the landform entropy of sub-basins in the study area (Fig. 10). The values of entropy and HI follow opposite trends. This finding represents two perspectives on the quantification of landform development, from the standpoint of residual material in the basin and the perspective of eroded material. The results of the correlation analysis between the HI values and the loess landform features show only a strong correlation between the HI values and the UEV. Therefore, the correlation between the two types of quantitative indicators and the UEV was also compared. The results are presented in Fig.11.

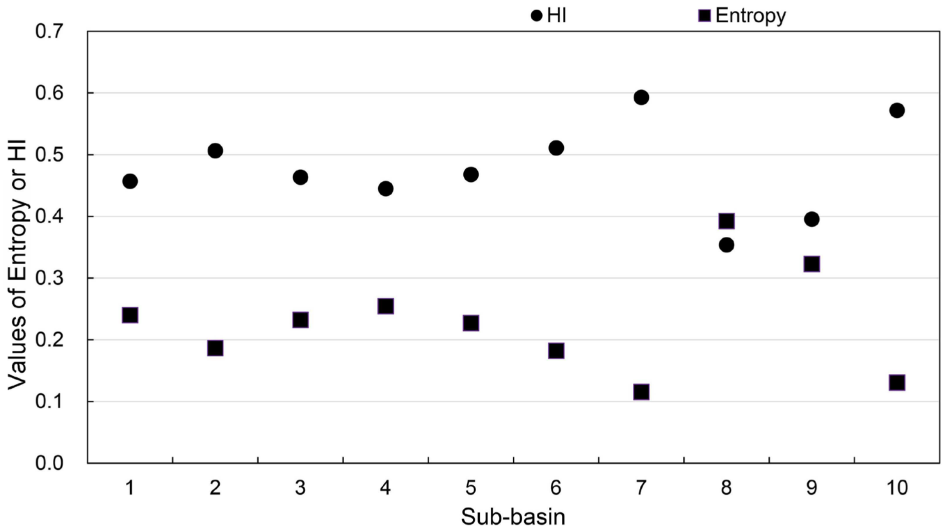

Fig. 10. Comparison of HI and entropy values in sub-basins

HI and entropy are correlated with UEV, more so for entropy (R^2=0.933). Although the theoretical basis of both indicators is W.M. Davis's (Davis, 1899) notion of a cycle of erosion, it is evident that the HI indicator has received more widespread attention, whilst the entropy indicator has only been applied to a small extent in the Chinese Loess Plateau. The entropy is a density function constructed based on the HI; thus, a certain correlation exists between entropy and HI. The distinction is that HI addresses a relatively closed landform system, whereas, in entropy theory, the concept of the landform as an open system was introduced. Ai and Yue (1988) concluded that the significance of entropy is not limited to the quantification of the landform development stage. The entropy value reflects the stage of landform development in a closed landform system (only influenced by internal forces), whilst the entropy value reflects the intensity of the interaction between internal and external forces in an open landscape system (influenced by internal and external forces) (Ai and Yue, 1988). In relation to the theoretical background of HI, some modifications have been made to the entropy to make them more relevant to the actual development of the landform, and more applications can be considered in future studies.

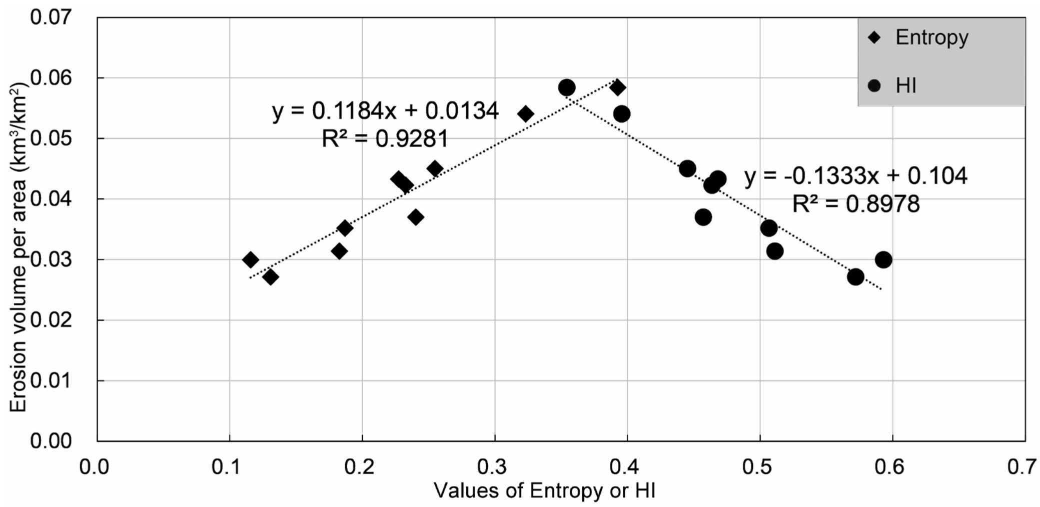

Fig. 11. Correlation between the two landform development indicators and UEV

5 Conclusions

This study applied the OBIA method to classify loess landforms in a basin within the Chinese Loess Plateau. It obtains excellent classification results with an accuracy of 88.7%. The quantitative results of landform development show that the HI values of all sub-basins are between 0.354 and 0.593, and the HI value of the entire basin is 0.486. This result indicates that the landform development of the whole basin is in the mature stage, following from severe surface erosion by gullying. Using quantitative indices based on terrain attributes, shape and pattern shows significant differences in the individual morphology and spatial distribution of the loess landform types. These differences are mainly reflected in area, shape complexity, length-width ratio, and spatial dispersion. These differences are likely to be caused by different gully erosion intensities during loess landform evolution and partially autogenic gully erosion. Meanwhile, we provide a basis for describing the morphology of the loess landform and monitoring large-scale loess gully changes, which can help comprehensively understand the development and evolution of the loess landforms.

Acknowledgments

The authors are grateful for the financial support provided by the National Natural Science Foundation of China (grant numbers 41930102, 41971333) and the University of Lausanne. Hong Wei also gives thanks to the China Scholarship Council. Many thanks are also given to the anonymous reviewers for their valuable and helpful comments.

Conflicts of interest

The authors declare no conflict of interest.

References

Ai, N., 1987. Comentropy in erosional-drainage-system. Journal of Soil Water Conservation, 1(2), 1-8 (in Chinese).

Ai, N., Yue, T., 1988. Second discussion of the comentropy of drainage-system. Journal of Soil Water Conservation, 4(2), 1-9 (in Chinese).

Antoniazza, G., Bakker, M., Lane, S. N., 2019. Revisiting the morphological method in two-dimensions to quantify bed-material transport in braided rivers. Earth Surf. Process. Landf 44(11), 2251-2267. https://doi.org/10.1002/esp.4633

Aplin, P., Smith, G. M., 2011. Introduction to object-based landscape analysis. International Int. J. Geogr. Inf. Sci 25(6), 869-875. https://doi.org/10.1080/13658816.2011.566570.

Arnold, J.G., Srinivasan, R., Muttiah, R.S., Williams, J.R., 1998. Large-area hydrologic modeling and assessment: Part I. Model development. J. Am. Water Resour. Assoc 34(1), 73-89. https://doi.org/10.1111/j.1752-1688.1998.tb05961.x.

Benz, U.C., Hofmann, P., Willhauck, G., Lingenfelder, I., Heynen, M., 2004. Multi-resolution, object-oriented fuzzy analysis of remote sensing data for GIS-ready information. ISPRS-J.

Photogramm. Remote Sens 58(3-4), 239-258. https://doi.org/10.1016/j.isprsjprs.2003.10.002.

Buyantuyev, A., Wu, J., 2007. Effects of thematic resolution on landscape pattern analysis. Landsc. Ecol 22(1), 7-13. https://doi.org/10.1007/s10980-006-9010-5.

Chen, C., Xie, G., Zhen, L., Leng, Y., 2008. Analysis on Jinghe watershed vegetation dynamics and evaluation on its relation with precipitation. Acta Ecologica Sinica, 28(3), 925-938 (in Chinese).

Chen, Y., Zhou, Y., Ge, Y., An, R., Chen, Y., 2018. Enhancing land cover mapping through integration of pixel-based and object-based classifications from remotely sensed imagery. Remote Sens. 10(1), 77. https://doi.org/10.3390/rs10010077.

Cheng, Y., Yang, X., Liu, H., Li, M., Rossiter, D.G., Xiong, L., Tang, G., 2020. Computer-assisted terrain sketch mapping that considers the geomorphological features in a loess landform. Geomorphology, 364, 107169. https://doi.org/10.1016/j.geomorph.2020.107169.

Crippen, R., Buckley, S., Belz, E., Gurrola, E., Hensley, S., Kobrick, M., Lavalle, M., Martin, J., Neumann, M., Nguyen, Q., 2016. NASADEM global elevation model: Methods and progress. http://hdl.handle.net/2014/46123.

Dai, W., Na, J., Huang, N., Hu, G., Yang, X., Tang, G., Xiong, L., Li, F., 2020. Integrated edge detection and terrain analysis for agricultural terrace delineation from remote sensing images. Int. J. Geogr. Inf. Sci 34(3), 484-503. https://doi.org/10.1080/13658816.2019.1650363.

Dai, W., Xiong, L., Antoniazza, G., Tang, G., Lane, S. N., 2021. Quantifying the spatial distribution of sediment transport in an experimental gully system using the morphological method. Earth Surf. Process. Landf 46(6), 1188-1208. https://doi.org/10.1002/esp.5094

Davis, W.M., 1899. The geographical cycle. The Geographical Journal, 14(5), 481-504. https://doi.org/1774538.

Ding, H., Liu, K., Chen, X., Xiong, L., Tang, G., Qiu, F., Strobl, J., 2020. Optimized segmentation based on the weighted aggregation method for loess bank gully mapping. Remote Sens. 12(5). https://doi.org/10.3390/rs12050793.

Ding, H., Na, J., Jiang, S., Zhu, J., Liu, K., Fu, Y., Li, F., 2021. Evaluation of three different machine learning methods for object-based artificial terrace mapping—a case study of the Loess Plateau, China. Remote Sens. 13(5), 1021. https://doi.org/10.3390/rs13051021.

Dingle, Robertson. L., King, D. J., 2011. Comparison of pixel-and object-based classification in land cover change mapping. Int. J. Remote Sens 32(6), 1505-1529. https://doi.org/10.1080/01431160903571791.

Drăguţ, L., Eisank, C., Strasser, T., 2011. Local variance for multi-scale analysis in geomorphometry. Geomorphology, 130(3-4), 162-172. https://doi.org/10.1016/j.geomorph.2011.03.011.

Drăguţ, L., Tiede, D., Levick, S.R., 2010. ESP: a tool to estimate scale parameter for multiresolution image segmentation of remotely sensed data. Int. J. Geogr. Inf. Sci 24(6), 859-871. https://doi.org/10.1080/13658810903174803.

Eger, A., Almond, P.C., Condron, L.M., 2012. Upbuilding pedogenesis under active loess deposition in a super-humid, temperate climate — quantification of deposition rates, soil chemistry and pedogenic thresholds. Geoderma, 189, 491-501. https://doi.org/10.1016/j.geoderma.2012.06.019.

Feng, L., Lin, H., Zhang, M., Guo, L., Jin, Z., Liu, X.J.E.G., 2020. Development and evolution of Loess vertical joints on the Chinese Loess Plateau at different spatiotemporal scales. Eng. Geol 265, 105372. https://doi.org/10.1016/j.enggeo.2019.105372.

Franke, R., 1982. Smooth interpolation of scattered data by local thin plate splines. Comput. Math. Appl 8(4), 273-281. https://doi.org/10.1016/0898-1221(82)90009-8.

Guan, Y., Yang, S., Zhao, C., Lou, H., Chen, K., Zhang, C., Wu, B., 2021. Monitoring long-term gully erosion and topographic thresholds in the marginal zone of the Chinese Loess Plateau. Soil Tillage Res 205, 104800. https://doi.org/10.1016/j.still.2020.104800.

Guo, J., Wang, W., Shi, J., 2015. A quantitative analysis of the stage of geomorphologic evolution in Luohe Drainage Basin, north of Shaanxi Province. Arid Land Geography, 38(6), 1162-1168 (in Chinese).

Hassett, E.M., Stehman, S.V., Wickham, J.D., 2012. Estimating landscape pattern metrics from a sample of land cover. Landsc. Ecol 27(1), 133-149. https://doi.org/10.1007/s10980-011-9657-4.

He, X., Tang, K., Zhang, X., 2004. Soil erosion dynamics on the Chinese Loess Plateau in the last 10,000 years. Mt. Res. Dev 24(4), 342-347. https://doi.org/10.1659/0276-4741(2004)024[0342:SEDOTC]2.0.CO;2.

He, Y., Chen, Y., Wang, W., Yan, H., Zhang, L., Liu, T., 2021. TS-InSAR analysis for monitoring ground deformation in Lanzhou New District, the loess Plateau of China, from 2017 to 2019. Adv. Space Res 67(4), 1267-1283. https://doi.org/10.1016/j.asr.2020.11.004.

Hu, G., Dai, W., Li, S., Xiong, L., Tang, G., Strobl, J., 2021. Quantification of terrain plan concavity and convexity using aspect vectors from digital elevation models.

Geomorphology, 375, 107553. https://doi.org/10.1016/j.geomorph.2020.107553.

Hu, S., Qiu, H., Wang, N., Cui, Y., Wang, J., Wang, X., Ma, S., Yang, D., Cao, M., 2020. The influence of loess cave development upon landslides and geomorphologic evolution: a case study from the northwest Loess Plateau, China. Geomorphology, 359, 107167. https://doi.org/10.1016/j.geomorph.2020.107167.

Huang, X., Tang, G., Zhu, T., Ding, H., Na, J., 2019. Space-for-time substitution in geomorphology. J. Geogr. Sci 29(10), 1670-1680. https://doi.org/10.1007/s11442-019-1684-0.

Irvin, B.J., Ventura, S.J., Slater, B.K., 1997. Fuzzy and isodata classification of landform elements from digital terrain data in Pleasant Valley, Wisconsin. Geoderma, 77(2-4), 137-154. https://doi.org/10.1016/S0016-7061(97)00019-0.

Jiang, C., Fan, W., Yu, N., Nan, Y., 2021. A new method to predict gully head erosion in the Loess Plateau of China based on SBAS-InSAR. Remote Sens. 13(3). https://doi.org/10.3390/rs13030421.

Johnson, B.A., Jozdani, S.E., 2018. Identifying generalizable image segmentation parameters for urban land cover mapping through meta-analysis and regression tree modeling. Remote Sens. 10(1). https://doi.org/10.3390/rs10010073.

Krummel, J.R., Gardner, R.H., Sugihara, G., O'Neill, R.V., Coleman, P.R.J.O., 1987. Landscape patterns in a disturbed environment. Oikos 48, 321-324. https://doi.org/3565520.

Lane, S.N., Richards, K.S., Chandler, J.H., 1993. Developments in photogrammetry; the geomorphological potential. Prog. Phys. Geogr. 17(3), 306-328. https://doi.org/10.1177/030913339301700302.

Li, C., Li, F., Dai, Z., Yang, X., Cui, X., Luo, L., 2020a. Spatial variation of gully development in the loess plateau of China based on the morphological perspective. Earth Sci. Inform 13(4), 1103-1117. https://doi.org/10.1007/s12145-020-00491-4.

Li, H., Wu, J., 2004. Use and misuse of landscape indices. Landsc. Ecol 19(4), 389-399. https://doi.org/10.1023/B:LAND.0000030441.15628.d6.

Li, J., Xiong, L., Tang, G., 2019. Combined gully profiles for expressing surface morphology and evolution of gully landforms. Front. Earth Sci 13(3), 551-562. https://doi.org/10.1007/s11707-019-0752-1.

Li, Q., Lu, Z., 1990. Quantitative study of the stage of geomorphological evolution. Acta Geographica Sinica, 45(1), 110-120 (in Chinese).

Li, S., Hu, G., Cheng, X., Xiong, L., Tang, G., Strobl, J., 2022. Integrating topographic knowledge into deep learning for the void-filling of digital elevation models. Remote Sens. Environ 269, 112818. https://doi.org/10.1016/j.rse.2021.112818.

Li, S., Xiong, L., Tang, G., Strobl, J., 2020b. Deep learning-based approach for landform classification from integrated data sources of digital elevation model and imagery. Geomorphology, 354, 107045. https://doi.org/10.1016/j.geomorph.2020.107045.

Lifton, N. A., Chase, C. G., 1992. Tectonic, climatic and lithologic influences on landscape fractal dimension and hypsometry: implications for landscape evolution in the San Gabriel Mountains, California. Geomorphology, 5(1-2), 77-114. https://doi.org/10.1016/0169-555X(92)90059-W.

Liu, K., Ding, H., Tang, G., Zhu, A.X., Yang, X., Jiang, S., Cao, J., 2017. An object-based approach for two-level gully feature mapping using high-resolution DEM and imagery: a case study on hilly loess plateau region, China. Chin. Geogr. Sci 27(3), 415-430. https://doi.org/10.1007/s11769-017-0874-x.

Liu, K., Na, J., Fan, C., Huang, Y., Ding, H., Wang, Z., Tang, G., Song, C., 2022a. Large-scale detection of the tableland areas and erosion-vulnerable hotspots on the Chinese Loess Plateau. Remote Sens, 14, 1946. https://doi.org/10.3390/rs14081946.

Liu, W., Zhang, H., Zhu, J., Hu, A., 2022b. Strategies for gully stabilization and highland protection in Chinese Loess Plateau. Front. Earth Sci. 10:812609. https://doi.org/10.3389/feart.2022.812609.

Liu, Y., Cao, J., Wang, L., Fang, X., Wagner, W., 2020. Regional features of topographic relief over the Loess Plateau, China: evidence from ensemble empirical mode decomposition. Front. Earth Sci 14(4), 695-710. https://doi.org/10.1007/s11707-020-0819-z.

Lu, H., Zhuo, H., Zhang, W., Wang, S., Zhang, H., Sun, X., Jia, X., Xu, Z., Wang, X., 2017. Earth surface processes and their effects on human behavior in monsoonal China during the Pleistocene-Holocene epochs. J. Geogr. Sci 27(11), 1311-1324. https://doi.org/10.1007/s11442-017-1437-x.

Luo, W., 1998. Hypsometric analysis with a geographic information system. Comput. Geosci 24(8), 815-821. https://doi.org/10.1016/S0098-3004(98)00076-4.

MacMillan, R., Pettapiece, W., Nolan, S., Goddard, T., 2000. A generic procedure for automatically segmenting landforms into landform elements using DEMs, heuristic rules and fuzzy logic. Fuzzy Sets Syst 113(1), 81-109. https://doi.org/10.1016/S0165-0114(99)00014-7.

McGarigal, K. 1995. FRAGSTATS: spatial pattern analysis program for quantifying landscape structure (Vol. 351). US Department of Agriculture, Forest Service, Pacific Northwest Research Station.

McGarigal, K., 2001. Landscape pattern metrics. Encyclopedia of Environmetrics. https://doi.org/10.1002/9780470057339.val006.pub2.

Meerkerk, A., van Wesemael, B., Bellin, N., 2009. Application of connectivity theory to model the impact of terrace failure on runoff in semi-arid catchments. Hydrol. Process 23(19), 2792-2803. https://doi.org/10.1002/hyp.7376.

Neel, M.C., McGarigal, K., Cushman, S.A., 2004. Behavior of class-level landscape metrics across gradients of class aggregation and area. Landsc. Ecol 19(4), 435-455. https://doi.org/10.1023/B:LAND.0000030521.19856.cb.

Nikfar, M., Zoej, M. J. V., Mohammadzadeh, A., Mokhtarzade, M., Navabi, A., 2012. Optimization of multiresolution segmentation by using a genetic algorithm. J. Appl. Remote Sens 6(1), 063592. https://doi.org/10.1117/1.JRS.6.063592.

Ohmori, H., 1993. Changes in the hypsometric curve through mountain building resulting from concurrent tectonics and denudation. Geomorphology, 8(4), 263-277. https://doi.org/10.1016/0169-555X(93)90023-U.

O'Neill, R.V., Krummel, J.R., Gardner, R.H., Sugihara, G., Jackson, B., DeAngelis, D.L., Milne, B.T., Turner, M.G., Zygmunt, B., Christensen, S.W., Dale, V.H., Graham, R.L., 1988. Indices of landscape pattern. Landsc. Ecol 1(3), 153-162. https://doi.org/10.1007/BF00162741.

Pérez-Peña, J.V., Azañón, J.M., Azor, A., 2009. CalHypso: An ArcGIS extension to calculate hypsometric curves and their statistical moments. Applications to drainage basin analysis in SE Spain. Comput. Geosci 35(6), 1214-1223. https://doi.org/10.1016/j.cageo.2008.06.006.

Pike, R.J., Wilson, S.E., 1971. Elevation-relief ratio, hypsometric integral, and geomorphic area-altitude analysis. GSA Bulletin, 82(4), 1079-1084. https://doi.org/10.1130/0016-7606(1971)82[1079:ERHIAG]2.0.CO;2.

Rahimi, E., Barghjelveh, S., Dong, P., 2021. Quantifying how urban landscape heterogeneity affects land surface temperature at multiple scales. Journal of Ecology and Environment, 45(1), 1-13. https://doi.org/10.1186/s41610-021-00203-z.

Shruthi, R.B.V., Kerle, N., Jetten, V., Abdellah, L., Machmach, I., 2015. Quantifying temporal changes in gully erosion areas with object oriented analysis. Catena, 128, 262-277. https://doi.org/10.1016/j.catena.2014.01.010.

Stevens, T., Carter, A., Watson, T.P., Vermeesch, P., Andò, S., Bird, A.F., Lu, H., Garzanti, E., Cottam, M.A., Sevastjanova, I., 2013. Genetic linkage between the Yellow River, the Mu Us desert and the Chinese Loess Plateau. Quat. Sci. Rev 78, 355-368. https://doi.org/10.1016/j.quascirev.2012.11.032.

Strahler, A.N., 1952. Hypsometric (area-altitude) analysis of erosional topography. Geol. Soc. Am. Bull 63(11), 1117-1142. https://doi.org/10.1130/0016-7606(1952)63[1117:HAAOET]2.0.CO;2.

Tang, G., Li, F., Liu, X., Long, Y., Yang, X., 2008. Research on the slope spectrum of the Loess Plateau. Sci. China Ser. E-Technol. Sci 51(1), 175-185. https://doi.org/10.1007/s11431-008-5002-9.

Tang, G., Song, X., Li, F., Zhang, Y., Xiong, L., 2015. Slope spectrum critical area and its spatial variation in the Loess Plateau of China. J. Geogr. Sci 25(12), 1452-1466. https://doi.org/10.1007/s11442-015-1245-0.

Tischendorf, L., 2001. Can landscape indices predict ecological processes consistently? Landsc. Ecol 16(3), 235-254. https://doi.org/10.1023/A:1011112719782.

Wang, J., Zhang, Y., Deng, J., Yu, S., Zhao, Y., 2021. Long-term gully erosion and its response to human intervention in the tableland region of the Chinese Loess Plateau. Remote Sens. 2021, 13, 5053. https://doi.org/10.3390/rs13245053.

Wang, X., Blanchet, F.G., Koper, N., 2014. Measuring habitat fragmentation: An evaluation of landscape pattern metrics. Methods Ecol. Evol 5(7), 634-646. https://doi.org/10.1111/2041-210X.12198.

Wang, Z., Jiao, J., Rayburg, S., Wang, Q., Su, Y., 2016. Soil erosion resistance of “Grain for Green” vegetation types under extreme rainfall conditions on the Loess Plateau, China. Catena, 141, 109-116. https://doi.org/10.1016/j.catena.2016.02.025.

Willgoose, G., Hancock, G., 1998. Revisiting the hypsometric curve as an indicator of form and process in transport‐limited catchment. Earth Surf. Process. Landf 23(7), 611-623. https://doi.org/10.1002/(SICI)1096-9837(199807)23:7<611::AID-ESP872>3.0.CO;2-Y.

Wei, H., Li, S., Li, C., Zhao, F., Xiong, L., Tang, G., 2021a. Quantification of loess landforms from three-dimensional landscape pattern perspective by using DEMs. ISPRS Int. J. Geo-Inf 10(10), 693. https://doi.org/10.3390/ijgi10100693.

Wei, H., Xiong, L., Tang, G., Strobl, J., Xue, K., 2021b. Spatial–temporal variation of land use and land cover change in the glacial affected area of the Tianshan Mountains. Catena, 202, 105256. https://doi.org/10.1016/j.catena.2021.105256.

Wu, H., Xu, X., Zheng, F., Qin, C., He, X., 2018. Gully morphological characteristics in the loess hilly-gully region based on 3D laser scanning technique. Earth Surf. Process. Landf 43(8), 1701-1710. https://doi.org/10.1002/esp.4332.

Wu, L., Yang, S., Liu, X., Luo, Y., Zhou, X., Zhao, H., 2014. Response analysis of land use change to the degree of human activities in Beiluo River basin since 1976. Acta Geographica Sinica, 69, 54-63 (in Chinese).

Wu, Q., Guo, F., Li, H., Kang, J., 2017. Measuring landscape pattern in three dimensional space. Landsc. Urban Plan 167, 49-59. https://doi.org/10.1016/j.landurbplan.2017.05.022.

Wu, Z., Wei, L., Lv, Z., 2012. Landscape pattern metrics: An empirical study from 2-D to 3-D. Phys. Geogr 33(4), 383-402. https://doi.org/10.2747/0272-3646.33.4.383.

Xiong, L., Tang, G., 2019. Spatial variations in loess landform inheritance. In Loess Landform Inheritance: Modeling and Discovery (pp. 169-204). Springer, Singapore.

Xiong, L., Tang, G., Li, F., Yuan, B., Lu, Z., 2014. Modeling the evolution of loess-covered landforms in the Loess Plateau of China using a DEM of underground bedrock surface. Geomorphology, 209, 18-26. https://doi.org/10.1016/j.geomorph.2013.12.009.

Xiong, L., Zhu, A., Zhang, L., Tang, G., 2018. Drainage basin object-based method for regional-scale landform classification: a case study of loess area in China. Phys. Geogr 39(6), 523-541. https://doi.org/10.1080/02723646.2018.1442062.

Xiong, L., Tang, G., Yang, X., Li, F., 2021. Geomorphology-oriented digital terrain analysis: Progress and perspectives. J. Geogr. Sci 31(3), 456-476. https://doi.org/10.1007/s11442-021-1853-9.

Yan, G., Mas, J.F., Maathuis, B., Xiangmin, Z., Van Dijk, P., 2006. Comparison of pixel-based and object-oriented image classification approaches—a case study in a coal fire area, Wuda, Inner Mongolia, China. Int. J. Remote Sens 27(18), 4039-4055. https://doi.org/10.1080/01431160600702632.

Yang, H., Wang, C., Ma, T., Guo, W., 2015. Accuracy assessment of interpolation methods in grid DEMs based on a variance-scale relation. Environ Earth Sci 74, 6525–6539. https://doi.org/10.1007/s12665-015-4388-5.

Yuan, S., Xu, Q., Zhao, K., Wang, X., Wang, C., 2020. Geomorphological classification and evolution of plateaubeam-loess hills in Heshui county of the east Gansu province. Geographical Research 39, 1920-1933 (in Chinese).

Zhang, H., Shi, Z., Fang, N., Guo, M., 2015. Linking watershed geomorphic characteristics to sediment yield: Evidence from the Loess Plateau of China. Geomorphology, 234, 19-27. https://doi.org/10.1016/j.geomorph.2015.01.014.

Zhang, L., Liang, S., Yang, X., Gan, W., 2020. Landscape evolution of the Eastern Himalayan Syntaxis based on basin hypsometry and modern crustal deformation. Geomorphology, 355, 107085. https://doi.org/10.1016/j.geomorph.2020.107085.

Zhang, T., Hu, Q., Fukuda, H., Zhou, D., 2016. The evaluation method of gully village's ecological sustainable development in the gully regions of Loess Plateau. Journal of Building Construction and Planning Research 4(01), 1-12. 10.4236/jbcpr.2016.41001.

Zhao S., Cheng W., 2014. Transitional relation exploration for typical loess geomorphologic types based on slope spectrum characteristics. Earth Surf. Dyn 2(2): 433-441. https://doi.org/10.5194/esurf-2-433-2014.

Zheng, J., Li, G., Han, Z., Meng, G., 2010. Hydrological cycle simulation of an irrigation district based on a SWAT model. Math. Comput. Model 51(11), 1312-1318. https://doi.org/10.1016/j.mcm.2009.10.036.

Zhou, Y., Yang, C., Li, F., Chen, R., 2021. Spatial distribution and influencing factors of Surface Nibble Degree index in the severe gully erosion region of China's Loess Plateau. J. Geogr. Sci 31, 1575–1597. https://doi.org/10.1007/s11442-021-1912-2.

Zhu, H., Zhao, Y., Liu, H., 2018. Scale characters analysis for gully structure in the watersheds of loess landforms based on digital elevation models. Front. Earth Sci 12, 431–443. https://doi.org/10.1007/s11707-018-0696-x.